

An efficient quantum algorithm for independent component analysis

Xiao-Fan Xu,^{1,2,3} Cheng Xue,^{4,*} Zhao-Yun Chen,⁴ Yu-Chun Wu,^{1,2,3,4,†} and Guo-Ping Guo^{1,2,3,4,5}

¹CAS Key Laboratory of Quantum Information, University of Science and Technology of China, Hefei 230026, China

²CAS Center for Excellence in Quantum Information and Quantum Physics,
University of Science and Technology of China, Hefei 230026, China

³Hefei National Laboratory, University of Science and Technology of China, Hefei 230088, China

⁴Institute of Artificial Intelligence, Hefei Comprehensive National Science Center, Hefei, Anhui, 230026, P. R. China

⁵Origin Quantum Computing Company Limited, Hefei, Anhui, 230026, P. R. China

Independent component analysis (ICA) is a fundamental data processing technique to decompose the captured signals into as independent as possible components. Computing the contrast function, which serves as a measure of independence of signals, is vital in the separation process using ICA. This paper presents a quantum ICA algorithm which focuses on computing a specified contrast function on a quantum computer. Using the quantum acceleration in matrix operations, we efficiently deal with Gram matrices and estimate the contrast function with the complexity of $O(\epsilon_1^{-2} \text{poly log}(N/\epsilon_1))$. This estimation subprogram, combined with the classical optimization framework, enables our quantum ICA algorithm, which exponentially reduces the complexity dependence on the data scale compared with classical algorithms. The outperformance is further supported by numerical experiments, while a source separation of a transcriptomic dataset is shown as an example of application.

I. INTRODUCTION

Independent component analysis (ICA) proposed during the 1990s [1–3] has nowadays become one of the fundamental techniques for data processing. Belonging to matrix factorization methods including the prominent principal component analysis (PCA), ICA manages to decompose data points into independent ingredients based mainly on statistical properties. The main motivation for the development of ICA techniques is at first the blind source separation (BSS) problem aimed at recovering latent variables from the observations. Researchers from fields including acoustics [4, 5], telecommunication [6], image processing [7, 8], biomedicine [9–12] started to introduce and address the BSS problem in a variety of contexts.

With the cocktail-party problem [13], it's convenient for one to intuitively understand what a BSS problem is like. Imagine that two people are speaking simultaneously around you. Amplitudes of speech signals from these speakers are denoted by $s_1(t)$ and $s_2(t)$, where t stands for time. You have two devices for recording. The recorded signal are then denoted by $x_1(t)$ and $x_2(t)$ which are naturally seen as a weighted sum of $s_1(t)$ and $s_2(t)$, written as

$$x_1(t) = a_{11}s_1 + a_{12}s_2, \quad (1)$$

$$x_2(t) = a_{21}s_1 + a_{22}s_2. \quad (2)$$

The BSS problem in this case is to recover the coefficients a_{ij} , and $s_i(t)$ as well, from only the observations $x_i(t)$.

As the most widely used method for the BSS problem, ICA won great success since it is realistic for the basic assumption that the underlying processes are mutually independent when they correspond to distinct physical processes. Under this assumption, observable random variables $\mathbf{x} = (x_1, x_2, \dots)^T$ are

arguably mixtures of some statistically independent "latent variables" $\mathbf{s} = (s_1, s_2, \dots)^T$. The linear mixture model is the most general choice which reads $\mathbf{x} = A\mathbf{s}$ with a coefficient matrix A . Algorithms that estimate A as well as \mathbf{s} came up successively mainly based on mutual information [3, 14–16], soon followed by algorithms involving more complex models such as linear convolutive mixtures [17] or nonlinear models [18].

An ICA algorithm typically proposes a contrast function that reflects the independence of a set of random variables, with the argument being their samples. The goal of the algorithm is to search for the linear mixtures of the samples that correspond to the extremum of the contrast function, perhaps by iteration or optimization. The scaling of any classical ICA algorithm is no less than the relevant problem size, which if we denote the sample size by N , can be referred to as $\Omega(N)$.

As restricted computing resources inevitably fall short of demands suggested by practical applications with large amounts of data, it is natural to turn to the prospective quantum computation which has shown a great advantage over the classical counterpart [19–25]. Furthermore, considering the strong correlation between ICA and PCA which can be exponentially accelerated by quantum PCA (qPCA) algorithm [26], this kind of quantum algorithm promisingly serves as a subroutine for ICA to leverage this acceleration.

Contrast functions based upon statistics including kurtosis and mutual information [27, 28] can be directly estimated using existing quantum estimators with a certain speedup [29, 30]. However, kurtosis is in general not robust, and even an optimal entropy estimator cannot provide satisfactory quantum speedup. We simply give relevant results in Appendix. A.

The Kernel ICA algorithm [31] owns a contrast function defined by the principal components of the Gram matrices constructed by samples. An adapted version of this function can be efficiently estimated with our quantum algorithm introduced in this paper. With given quantum access to the samples, our algorithm starts by encoding the Gram matrices onto

* xcheng@iai.ustc.edu.cn

† wuyuchun@ustc.edu.cn

amplitudes of a quantum state. By the parallel execution of two eigenvalue estimation circuits, the principal components of Gram matrices are extracted, measured, and used for the computation of the contrast function. As this step is the main bottleneck of the computation, it provides a critical speedup for the overall KICA. For sample size N , the complexity of performing ICA with our method scales as $O(\text{poly log}(N))$, exponentially faster than its classical counterpart.

The adaptation of the contrast function is to circumvent restrictions imposed by the quantum measurement. The problem may arise that the adapted function fails to give the correct independence of its input so that even when it approaches the extremum, separated results are not independent at all. However, we numerically verify its feasibility for source separation (including comparing the adapted and the original contrast function). We also give a rigorous error analysis for the output and explain that a linear separation of non-Gaussian variables is feasible. Numerical experiments are presented to verify the ability of separation and error performance of our algorithm. Furthermore, we numerically simulate the source separation process on a transcriptomic dataset as an illustration of applications.

The remainder of this paper is organized as follows: Section II lists the relevant conceptions of ICA and introduces the KICA algorithm. We describe our method adapted from KICA and present a theoretical analysis in Section III. Numerical experiments of our algorithm are shown in Section IV. In Section V we give a conclusion and further discussion.

II. INDEPENDENT COMPONENT ANALYSIS: CONCEPTIONS AND ALGORITHM

In this section, we briefly recall conceptions of ICA and basic preprocessing techniques. Then we introduce the KICA algorithm as a background of our work.

A. ICA

We take the linear ICA model for a rigorous definition of ICA [13].

Definition 1 (ICA). Assume that m observable random variables $\mathbf{x}_1, \mathbf{x}_2, \dots, \mathbf{x}_m$ can be modeled as linear mixtures of m independent components (ICs) with real coefficients A_{ij} :

$$\mathbf{x}_j = A_{j1}\mathbf{s}_1 + A_{j2}\mathbf{s}_2 + \dots + A_{jm}\mathbf{s}_m, \quad (3)$$

where "IC" means these unknown s_i are statistically independent. We use the notation that $\mathbf{x} = (\mathbf{x}_1, \mathbf{x}_2, \dots, \mathbf{x}_m)^T$, $\mathbf{s} = (\mathbf{s}_1, \mathbf{s}_2, \dots, \mathbf{s}_m)^T$ and matrix \mathbf{A} with entries A_{ij} . ICA is to estimate \mathbf{A} together with ICs \mathbf{s} with only samples of \mathbf{x} .

To avoid ambiguity, we denote the j -th of all N samples of \mathbf{x}_i by x_{ij} , and define vectors $\mathbf{x}_i = (x_{i1}, x_{i2}, \dots, x_{iN})^T$ and matrix $X = (x_1, x_2, \dots, x_m)^T$, similarly for s_{ij}, s_i, S . Bold used or not is to distinguish between variables and samples.

To assess the independence of a set of random variables \mathbf{x}_i given samples X , the so-called contrast function was put forward [28]. In this paper, a contrast function is denoted by $J(X)$, with input samples X and output reflecting the independence of these variables. Choices of contrast functions vary as different ICA algorithms are considered [14, 16, 31]. A contrast function is kind of a separation criterion that determines how independent we perceive \mathbf{x}_i to be. Given a linear transformation \mathbf{W} , $\mathbf{x}' = \mathbf{W}\mathbf{x}$ is considered as more independent if $J(\mathbf{W}X) \leq J(X)$. It is naturally expected that the contrast function reaches its extremum when $\mathbf{W} = \mathbf{A}^{-1}$ so that a solution to ICA is obtained. A basic process of an ICA algorithm is to search for the optimal \mathbf{W} according to $J(\mathbf{W}X)$ by optimization or iteration. In practice the optimized \mathbf{W} is seen as an estimation of \mathbf{A}^{-1} , thus ICs $S = \mathbf{W}X$ are estimated.

Throughout this paper, we take the assumption that x_i, s_i are real and share the same length for simplicity, and in addition, \mathbf{s} are zero-mean and unit-variance. The independence demands the covariance matrix of \mathbf{s} equal the identity. As \mathbf{s} are zero mean, this can be written as $E\{\mathbf{s}\mathbf{s}^T\} = \mathbf{I}$, where $E\{\cdot\}$ represents expectation and $E\{\mathbf{s}\mathbf{s}^T\}$ is the matrix with entries $E\{s_i s_j\}$. The assumption concretely reads

$$E\{s_i s_j\} = \begin{cases} 0, & i = j, \\ 1, & i \neq j. \end{cases} \quad (4)$$

That the inverse of coefficient matrix \mathbf{A}^{-1} exists is also assumed, so that we can write

$$\mathbf{s} = \mathbf{A}^{-1}\mathbf{x} \quad (5)$$

for later discussion.

B. Preprocessing

Considering preprocessing before applying the ICA algorithm always makes the problem simpler and better conditioned. Especially, techniques like centering and whitening are almost necessary steps for ICA.

Centering means making samples x_i zero-mean by subtracting its expectation $x_{ij} - E\{x_i\}$, where the expectation is in general estimated by the sample mean. Though Eq. eq3 has implied that \mathbf{x}_j is zero-mean, by whitening ICA also works in the non-zero mean case.

Suppose \mathbf{x}_i itself has been centered, whitening is to transform X into samples of 'whitened' variables \mathbf{y} so that the covariance matrix of \mathbf{y} equals the identity matrix: $E\{\mathbf{y}\mathbf{y}^T\} = \mathbf{I}$. Whitening is always possible by computing the eigendecomposition of the covariance matrix: $E\{\mathbf{x}\mathbf{x}^T\} = \mathbf{E}\mathbf{D}\mathbf{E}^T$, where \mathbf{E} and \mathbf{D} are matrices composed of eigenvectors and eigenvalues, respectively. Then it is easy to check that

$$\mathbf{y} = (E\{\mathbf{x}\mathbf{x}^T\})^{-1/2}\mathbf{x} = \mathbf{E}\mathbf{D}^{-1/2}\mathbf{E}^T\mathbf{x} = \mathbf{E}\mathbf{D}^{-1/2}\mathbf{E}^T\mathbf{A}\mathbf{s}, \quad (6)$$

leads to

$$E\{\mathbf{y}\mathbf{y}^T\} = \mathbf{I}. \quad (7)$$

By assuming that $E\{\mathbf{ss}^T\} = \mathbf{I}$, it's evident that the coefficient matrix $\mathbf{E}\mathbf{D}^{-1/2}\mathbf{E}^T\mathbf{A}$ is orthogonal.

Substitute these statistics by sample mean:

$$Y = \mathbf{E}\mathbf{D}^{-1/2}\mathbf{E}^T X = \mathbf{E}\mathbf{D}^{-1/2}\mathbf{E}^T \mathbf{A}\mathbf{S}, \quad (8)$$

where we can regard Y as samples of \mathbf{y} . Note that Y differs from S by only an orthogonal transformation. Therefore, whitening makes it suffice to search through orthogonal matrices only for the optimal $\mathbf{W} = (\mathbf{E}\mathbf{D}^{-1/2}\mathbf{E}^T\mathbf{A})^{-1}$ if we replace X by Y .

C. KICA

Among all the ICA algorithms, KICA, which we will introduce in a second, appears to be numerically relatively robust [31] and related closely to matrix operations. As introduced before, KICA minimizes its contrast function for \mathbf{W} by optimization for estimation of \mathbf{A}^{-1} .

The contrast function is determined and can be computed after selecting a kernel function $K(x, y)$, e.g. a Gaussian kernel we use later:

$$K(x, y) = \exp\left\{-\frac{|x-y|^2}{2\sigma^2}\right\}. \quad (9)$$

The contrast function is computed by the following four steps, which can be considered roughly as its definition.

Step 1: Compute K_i with selected kernel function $K(x, y)$ and samples X :

$$(\tilde{K}_i(X))_{jk} = K(x_{ij}, x_{ik}), \quad (10)$$

$$K_i(X) = (\mathbf{I} - \mathbf{1}/N)\tilde{K}_i(\mathbf{I} - \mathbf{1}/N), \quad (11)$$

where \tilde{K}_i (K_i) is called (centered) Gram matrix, respectively. Variables in parentheses specify the input samples. In this paper, the Gram matrices we used generally refer to the centered one in the absence of a specific designation. We denote the matrix with all entries 1 by $\mathbf{1}$ and the identity matrix by \mathbf{I} .

Step 2: Perform an eigenvalue decomposition for all Gram matrices:

$$K_i(X) = U_i \Lambda_i U_i^T. \quad (12)$$

Denote the k -th eigenvalue of K_i by λ_{ik} and corresponding eigenvectors by \tilde{u}_{ik} . U_i and Λ_i are defined as $U_i = (\tilde{u}_{i1}, \tilde{u}_{i2}, \dots, \tilde{u}_{iN})$ and $\Lambda_i = \text{diag}(\lambda_{i1}, \lambda_{i2}, \dots, \lambda_{iN})$, respectively.

Based upon the conclusion that only $M_i = O(\log N)$ largest eigenvalues make sense for Gaussian kernel [31, 32], an approximated decomposition can be used instead which is given by $K_i \approx \tilde{U}_i \tilde{\Lambda}_i \tilde{U}_i^T$, for $\tilde{U}_i = (\tilde{u}_{i1}, \tilde{u}_{i2}, \dots, \tilde{u}_{iM_i})$ and $\tilde{\Lambda}_i = \text{diag}(\lambda_{i1}, \lambda_{i2}, \dots, \lambda_{iM_i})$.

Step 3: Choose a positive constant κ , and then compute the positive-definite matrix \mathcal{R}_κ :

$$\mathcal{R}_\kappa(X) = \begin{pmatrix} \mathbf{I} & R_1 U_1^T U_2 R_2 & \cdots & R_1 U_1^T U_m R_m \\ R_2 U_2^T U_1 R_1 & \mathbf{I} & \cdots & R_2 U_2^T U_m R_m \\ \vdots & \vdots & \ddots & \vdots \\ R_m U_m^T U_1 R_1 & R_m U_m^T U_2 R_2 & \cdots & \mathbf{I} \end{pmatrix}, \quad (13)$$

where $R_i = \text{diag}(\lambda'_{i1}, \lambda'_{i2}, \dots, \lambda'_{iM_i})$ with the notation that $\lambda'_{ik} = \lambda_{ik}/(\lambda_{ik} + \kappa)$.

Step 4: Compute the determinant of \mathcal{R}_κ , $\det(\mathcal{R}_\kappa)$, and contrast function is taken as $J(X) = -\ln(\det(\mathcal{R}_\kappa))$.

We have introduced the overall computational process for contrast function $J(X)$ hereinbefore. The only job left is to perform optimization with $J(X)$. Moreover, as we have discussed in the last section, by replacing X with whitened Y , the problem is reduced to an optimization for an orthogonal matrix, which is the optimization problem on the Stiefel manifold with relatively mature techniques to deal with [33].

III. QUANTUM ALGORITHM FOR ADAPTED KICA

ICA algorithms like KICA, based mainly on matrix operations, may achieve better quantum speedup. Different from the original KICA, we replace the contrast function by R_κ to circumvent the restrictions of measurements, where R_κ is defined as the element-wise absolute values of \mathcal{R}_κ . We introduce a quantum algorithm to compute $J(\mathbf{W}Y) = \det(R_\kappa(\mathbf{W}Y))$ in this section. We use the following notations that $X = (x_1, x_2, \dots, x_m)^T$, $X' = (x'_1, x'_2, \dots, x'_m)^T$, $Y = (y_1, y_2, \dots, y_m)^T$ respectively represents the original, centered and preprocessed samples and another one that $\mathbf{W}Y = (y'_1, y'_2, \dots, y'_m)^T$.

A. Main results

The problem to be solved on a quantum computer is stated in Problem 1:

Problem 1 (Computation of contrast function). *Given N samples x_i of each of the m random variables \mathbf{x}_i . Suppose we have the oracle access to x_i : $O_{x_i}|j\rangle|0\rangle = |j\rangle|x_{ij}\rangle$, where $|x_{ij}\rangle$ is an s -bit binary string representing x_{ij} by qubits. The target is to estimate $\det(R_\kappa(\mathbf{W}Y))$ for some orthogonal \mathbf{W} with only elementary gates and queries to O_{x_i} .*

Denote the centered kernel by

$$K'(y, x) = K(y, x) - \int_{\mathbb{R}} d\rho_{z_i}(\alpha)K(\alpha, x) - \int_{\mathbb{R}} d\rho_{z_i}(\beta)K(y, \beta) + \int_{\mathbb{R}^2} d\rho_{z_i}(\alpha)d\rho_{z_i}(\beta)K(\alpha, \beta). \quad (14)$$

In our analysis, we require y'_i to satisfy

$$\int_{\mathbb{R}} K'(y'_{im}, x)g(x)f_{y'_i}(x)dx = \frac{1}{N} \sum_{n=1}^N (K_i)_{mn}g(y'_{im}), \quad (15)$$

for all i, m , arbitrary \mathbf{W} and any function $g \in L^2(\mathbb{R})$, where $f_{y'_i}(x)$ is the probability density function (PDF) of y'_i . Under the commonly used assumption that the distribution of \mathbf{x}_i is exactly one of obtained samples, this condition is naturally satisfied.

The oracle O_{x_i} may be provided by qRAM [34], which allows this state preparation within $O(\text{poly log } N)$ operations.

Using oracles, we estimate the covariance matrix M of \mathbf{X} and then execute the preprocessing subprogram, where the estimation is denoted by \tilde{M} . This causes the input error so that the final output estimates $R_\kappa(\mathbf{W}\tilde{Y})$ instead. Denote by μ_M the condition number of M . The input error can then be expressed as

$$\tilde{y}_{ij} = \sum_{k=1}^m (\tilde{M}^{-\frac{1}{2}})_{ik} (x_{kj} - E\{\mathbf{x}_k\}), \quad (16)$$

and

$$\|\tilde{M}^{-\frac{1}{2}} - M^{-\frac{1}{2}}\|_2 < \varepsilon_2. \quad (17)$$

The main result of our method for Problem 1 is stated as Theorem 1.

Theorem 1. *Denote by $d = \Theta(m \log N)$ and ξ the dimension and the minimal eigenvalue of $R_\kappa(\mathbf{W}\tilde{Y})$. Given $\varepsilon_1 < \frac{1}{d^2}$, $\varepsilon_2 < 0.2$ and κ , and samples x_i with size N of m random variables \mathbf{x}_i together with oracles access to x_i , $O_{x_i}|j\rangle|0\rangle = |j\rangle|x_{ij}\rangle$, there exists a quantum algorithm outputting $\det(\tilde{R}_\kappa(\mathbf{W}\tilde{Y}))$, where*

$$\frac{|\det(\tilde{R}_\kappa(\mathbf{W}\tilde{Y})) - \det(R_\kappa(\mathbf{W}\tilde{Y}))|}{\det(R_\kappa(\mathbf{W}\tilde{Y}))} = \tilde{O}(\varepsilon_1), \quad (18)$$

using $\tilde{O}(\frac{1}{\xi^2 \varepsilon_1^2} + \frac{\mu_M^2}{\varepsilon_2 \|M\|_2^{3/2}})$ elementary gates and queries to each O_{x_i} .

We neglect factors in m , κ and use \tilde{O} to denote the complexity up to polylogarithmic factors in N , ε_1 , ε_2 , μ_M . It is worth noting that ξ is usually $O(1)$ during our tests when appropriately choosing κ , for example, to be 0.1.

Further analysis of the special case is given in Theorem 2, that $\mathbf{y}' = \mathbf{W}\tilde{\mathbf{y}}$ has few mutual dependence (called near-independent case later), where a better complexity can be achieved.

Theorem 2. *Continue with the notation of Theorem 1, but require that $\varepsilon_1 < 1$, $\varepsilon_2^2 \ll \varepsilon_2 = o(d^{-2})$ instead. When*

$$\tilde{\mathbf{y}}' = (1 + \varepsilon_2 F)\mathbf{s} + o(\varepsilon_2^2), \quad (19)$$

where $\|F\|_{\max} \leq 1$ is assumed, the precision of output can be changed into:

$$\frac{|\det(\tilde{R}_\kappa(\mathbf{W}\tilde{Y})) - \det(R_\kappa(\mathbf{W}\tilde{Y}))|}{\det(R_\kappa(\mathbf{W}\tilde{Y}))} = \tilde{O}(\varepsilon_1 \varepsilon_2), \quad (20)$$

with the query and gate complexity of $\tilde{O}(\frac{1}{\varepsilon_1^2 \varepsilon_2} + \frac{\mu_M^2}{\varepsilon_2 \|M\|_2^{3/2}})$.

The main idea of our method is that, we first construct the circuit $O_{y'_i}|j\rangle|0\rangle = |j\rangle|y'_{ij}\rangle$ by a quantum preprocessing subprogram, then manage to encode the Gram matrix $K_i(\mathbf{W}\mathbf{Y})$ onto a quantum state, and finally by quantum circuits and quantum measurements, we obtain the classical information to reconstruct the low dimensional $R_\kappa(\mathbf{W}\mathbf{Y})$ together with its determinant. The preprocessing subprogram and function estimation are respectively introduced in Section III B and Section III C. We summarize our method for the near-independent case in Algorithm 1, and the general one can be obtained by slight modification. A flow chart is shown in Fig. 1 including optimization discussed in Section III D.

Algorithm 1: Computation of the contrast function.

- 1 **Input:** Near-independent samples X , Sample size N , state preparation oracles O_{x_i} , parameterized matrix \mathbf{W} , kernel function $K(x, y)$, preselected parameter κ , error tolerance ε_1 , ε_2 .
 - 2 **Output:** $\det(\tilde{\mathcal{R}}_\kappa(\mathbf{W}\tilde{Y}))$ with multiplicative error of $\tilde{O}(\varepsilon_1 \varepsilon_2)$ and $\sqrt{\sum_{i=1}^m (\tilde{y}'_{ij} - y'_{ij})^2} < \varepsilon_2$.
 - 3 **Runtime:** $\tilde{O}(\frac{1}{\varepsilon_1^2 \varepsilon_2} + \frac{\mu_M^2}{\varepsilon_2 \|M\|_2^{3/2}})$ uses of oracles O_{x_i} and its inverse, and elementary quantum gates.
 - 4 **Procedure::**
 - 5 Compute the covariance matrix M of \mathbf{x} ;
 - 6 Use M to construct the state preparation $O_{y'_i}$ for every i , and set $\mathbf{z} = \mathbf{y}'$;
 - 7 **foreach** $0 \leq i < m$ **do**
 - 8 **for** $k = 1, 2, \dots, K = \tilde{O}(1/\varepsilon_1)$ **do**
 - 9 Use the circuit O_{ε_1} to prepare $|\phi_{\varepsilon_1}\rangle$;
 - 10 Measure the last register for λ_{ik}/N ;
 - 11 **end**
 - 12 **end**
 - 13 **foreach** $0 \leq i < j < m$ **do**
 - 14 **foreach** $\tilde{\lambda}_{ik}$ and $\tilde{\lambda}_{jl}$ measured **do**
 - 15 Use the amplitude estimation with U_{ε_1} for overlaps between $|\psi_{\varepsilon_1}\rangle$ and $|\tilde{\lambda}_{ik}, \tilde{\lambda}_{jl}\rangle$;
 - 16 **end**
 - 17 **end**
 - 18 Calculate the contrast function using the measured values.
-

B. Preprocessing on a quantum computer

The preprocessing subprogram has three steps: Step 1: use the quantum mean estimator for the covariance matrix M of \mathbf{x} ; step 2: classically compute the mixing coefficients, $\mathbf{W}M^{-1/2}$; step 3: use controlled weighted sum algorithm introduced in [35] to linearly transform O_{x_i} into $O_{y'_i}$. The formal result is stated in Lemma 1.

Lemma 1. *Given oracles $O_{x_i} : |j\rangle|0\rangle \rightarrow |j\rangle|x_{ij}\rangle$ when $\max_{i,j} \{|x_{ij} - E\{\mathbf{x}_i\}|\} \leq 1$ is assumed, sample means $E\{x_i\}$ and the covariance matrix M can be estimated within $\tilde{O}(\frac{\mu_M^2 m}{\|M\|_2^{3/2} \varepsilon})$ gates and queries to O_{x_i} , so that the estimated $\tilde{M}^{-\frac{1}{2}}$ satisfies that*

$$\|\tilde{M}^{-\frac{1}{2}} - M^{-\frac{1}{2}}\|_2 < \varepsilon, \quad (21)$$

where μ_M is the condition number of M . With such estimation, $O_{y'_i}$ can be executed with $O(\text{poly log}(\frac{N}{\varepsilon}))$ gates and queries to O_{x_i} , where

$$O_{y'_i}|j\rangle|0\rangle = |j\rangle|y'_{ij}\rangle. \quad (22)$$

We have

$$\tilde{y}'_{ij} = \sum_{k=1}^m (\mathbf{W}\tilde{M}^{-\frac{1}{2}})_{ik} (x_{kj} - \tilde{E}\{\mathbf{x}_k\}). \quad (23)$$

Proof. The preprocessing has 2 phases, where the former estimates the covariance matrix and the latter utilizes the acquired knowledge for state preparation.

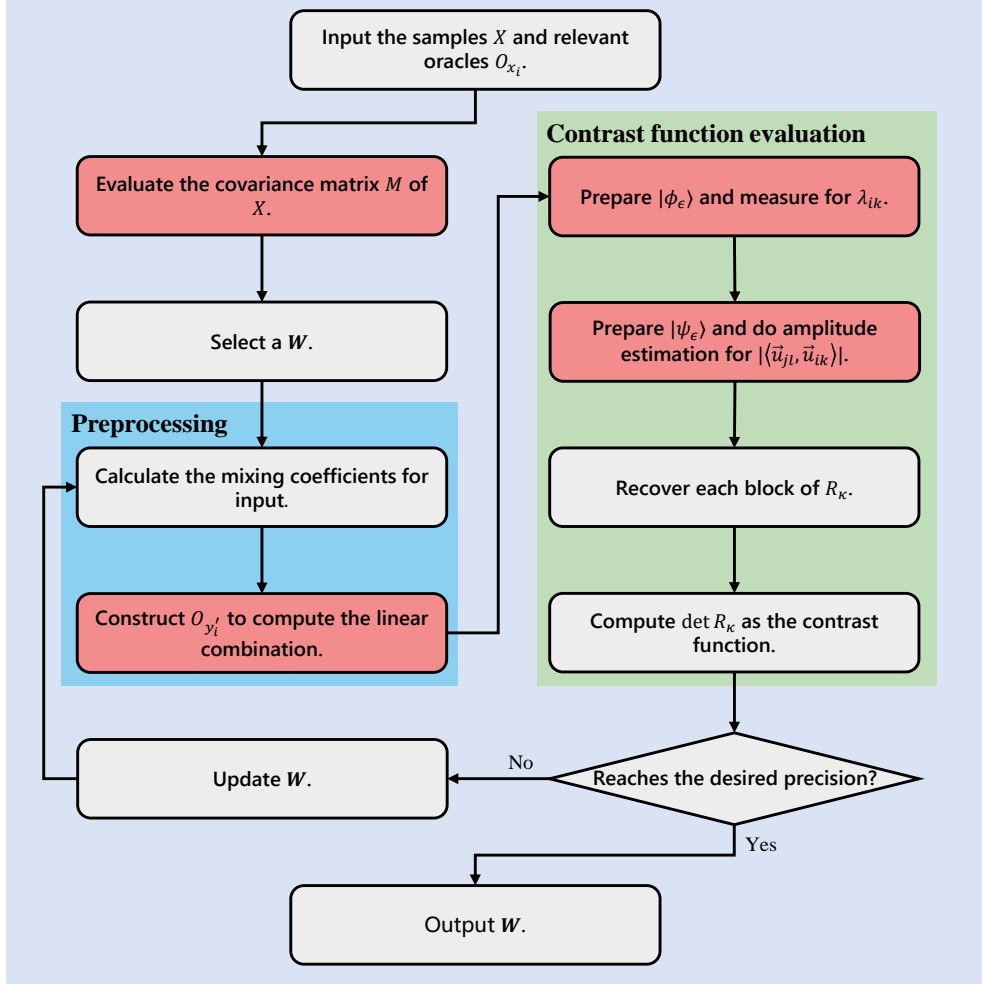


FIG. 1: A flowchart outlining the process for optimizing to obtain the optimal unmixing coefficients \mathbf{W} , where the red block implies the procedure using a quantum computer.

For the first phase, we use a quantum mean estimator proposed in [29], which, for example, outputs the mean of x_i using oracles such as O_{x_i} with gate and query complexity of $\tilde{O}(1/\epsilon)$. Ignore the error induced by quantum arithmetics [35], by which we can construct $O_{x_i x_j} : |k\rangle|0\rangle \rightarrow |k\rangle|x_{ik}x_{jk}\rangle$. With O_{x_i} and $O_{x_i x_j}$, both $E\{x_i\}$ and $E\{x_i x_j\}$ are estimated with accuracy of $\frac{\|M\|_2^{3/2}\epsilon}{8\mu_M^2 m}$. Therefore, M can be estimated since $Cov(x_i, x_j) = E\{x_i x_j\} - E\{x_i\}E\{x_j\}$. The gate and query complexity of the computation of coefficients is eventually $\tilde{O}\left(\frac{\mu_M^2 m}{\|M\|_2^{3/2}\epsilon}\right)$ [29].

Thus, calculate the coefficient matrix $\mathbf{W}M^{-1/2}$ classically using acquired M . Through the process of controlled weighted sum [35] to linear combine x_i on a quantum register, O_{y_i} in Eq. 22 is constructed. Both query and gate complexity of O_{y_i} is $O(\text{poly log}(N/\epsilon))$. The error bound of M is proved in Appendix B 1.

C. Evaluation of the contrast function

Here we start to introduce a quantum circuit computing $J(Z)$ for general input more than just $\mathbf{W}Y$ with queries to oracles $O_{z_i}, i = 1, 2, \dots, m$. We use five subprocedures to achieve this goal. The first one is to construct an oracle \tilde{O}_{K_i} outputting entries of uncentered Gram matrix $\tilde{K}_i(Z)$, where

$$\tilde{O}_{K_i}|j\rangle|k\rangle|z\rangle \rightarrow |j\rangle|k\rangle|z\rangle \oplus (\tilde{K}_i)_{jk}. \quad (24)$$

The second is to block encode the centered Gram matrix $K_i(Z)$, with the corresponding circuit named U_{K_i} . With U_{K_i} , an eigenvalue estimation circuit $U_i : |u_{ik}\rangle|0\rangle \rightarrow |u_{ik}\rangle|\lambda_{ik}/N\rangle$ based on phase estimation can be constructed, where

$$|u_{ik}\rangle = \sum_{\alpha=1}^N (\bar{u}_{ik})_{\alpha} |\alpha\rangle, \quad (25)$$

and $\lambda_{ik}, \bar{u}_{ik}$ are k -th eigenvalue, normalized eigenvector of $K_i(Z)$. The third subprocedure is to implement U_i and U_j par-

□

allely on the initial state $|K_i\rangle|0\rangle|0\rangle$, where

$$|K_i(Z)\rangle = \frac{1}{N} \sum_{j,k=1}^N (K_i)_{jk} |j\rangle|k\rangle. \quad (26)$$

shown in Fig. 4. The output is about

$$\sum_{k,l=1}^N \frac{\lambda_{ik}}{N} \langle \vec{u}_{jl}, \vec{u}_{ik} | u_{ik} \rangle |u_{jl}\rangle |\lambda_{ik}/N\rangle |\lambda_{jl}/N\rangle + |\perp\rangle, \quad (27)$$

for $|\perp\rangle$ being the state of no interest to us. By quantum measurement and amplitude estimation, we obtain the values of λ_{ik}/N and $|\langle \vec{u}_{jl}, \vec{u}_{ik} \rangle|$ and then compute $R_\kappa(Z)$ by

$$(R_\kappa)_{ik,jl} = \frac{\lambda_{ik}/N}{\lambda_{ik}/N + \kappa/2} \frac{\lambda_{jl}/N}{\lambda_{jl}/N + \kappa/2} |\langle \vec{u}_{ik}, \vec{u}_{jl} \rangle|. \quad (28)$$

The process of measurement is called the fourth step while the classical computation of $R_\kappa(Z)$ as well as its determinant $J(Z)$ is called the fifth.

Now we give details of each subprocedure. Step 1 is to use quantum operations following the route below:

$$\begin{aligned} |j, k, 0, 0, 0\rangle &\rightarrow |j, k, z_{ij}, z_{ik}, 0\rangle \\ &\rightarrow |j, k, z_{ij}, z_{ik}, K(z_{ij}, z_{ik})\rangle \\ &\rightarrow |j, k, 0, 0, K(z_{ij}, z_{ik})\rangle \end{aligned} \quad (29)$$

where the 3 operations are respectively queries to O_{z_i} , quantum arithmetics and the inverse $O_{z_i}^\dagger$. This is formally stated in Lemma 2, while proofs of lemmas in this section are left to Appendix. C.

Lemma 2. *The quantum circuit, $\tilde{O}_{K_i} : |j\rangle|k\rangle|z\rangle \rightarrow |j\rangle|k\rangle|z \oplus K(z_{ij}, z_{ik})\rangle$, can be constructed using $O(\text{polylog}(N/\varepsilon))$ quantum gates and 2 queries to both O_{z_i} and $O_{z_i}^\dagger$.*

The block-encoding of $K_i(Z)$ introduced in the second subprocedure is given in Lemma 3.

Lemma 3. *An $(N, n + s + 1, \varepsilon)$ -block-encoding of $\tilde{K}_i(Z)$, \tilde{U}_{K_i} is given by*

$$\begin{aligned} \tilde{U}_{K_i} = & (\text{SWAP}_n \otimes I_{s+1}) (I_n \otimes H^{\otimes n} \otimes I_{s+1}) (\tilde{O}_{K_i}^\dagger \otimes I_1) \\ & (I_{2n} \otimes \text{CR}) (\tilde{O}_{K_i} \otimes I_1) (I_n \otimes H^{\otimes n} \otimes I_{s+1}), \end{aligned} \quad (30)$$

where I_n and SWAP_n respectively represent the n -qubit identity operator and swap gate, and we define $\text{CR} : |a\rangle|0\rangle \rightarrow |a\rangle(a|0\rangle + \sqrt{1-a^2}|1\rangle)$. An $(N, n + s + 2, \varepsilon)$ -block-encoding of $K_i(Z)$ is then given by $U_{K_i} = C_{\Pi} \text{NOT} \cdot \tilde{U}_{K_i} \cdot C_{\Pi} \text{NOT}$, using $O(\text{polylog}(N/\varepsilon))$ quantum gates and one query to \tilde{O}_{K_i} and its inverse. We define

$$\Pi = (I_n - |\vec{1}\rangle\langle\vec{1}|) \otimes |0^{\otimes n+s+1}\rangle\langle 0^{\otimes n+s+1}|, \quad (31)$$

for the uniform superposition state denoted by $|\vec{1}\rangle$, and

$$C_{\Pi} \text{NOT} = \Pi \otimes X + (I - \Pi) \otimes I. \quad (32)$$

They give

$$\langle j, 0^{\otimes n+s+1}, 1 | U_{K_i} | k, 0^{\otimes n+s+1}, 1 \rangle = \frac{(K_i)_{jk}}{N}. \quad (33)$$

The block-encoding circuit is illustrated in Fig. 2, with $C_{\Pi} \text{NOT}$ shown in Fig. 3a. The Quantum singular value transformation (QSVT) technique [36] then allows the block-encoding of the evolution operator $e^{iK_i t/N}$. A phase estimation of $e^{iK_i t/N}$ gives the eigenvalue estimation circuit U_i introduced at the beginning of this section, which is illustrated in Fig. 3b and analyzed in Lemma 4.

Lemma 4. *Given $0 < \varepsilon < 1$, the eigenvalue estimation circuit U_i :*

$$|u_{ik}\rangle|0\rangle \rightarrow |u_{ik}\rangle \left| \frac{\tilde{\lambda}_{ik}}{N} \right\rangle, \quad (34)$$

can be implemented using $\tilde{O}(\frac{1}{\varepsilon})$ queries to U_{K_i} and elementary gates, where $|\lambda_{ik} - \tilde{\lambda}_{ik}| \leq N\varepsilon$.

The circuit of the third subprocedure is illustrated in Fig. 4, where two eigenvalue estimation circuits are implemented. Projections $\Pi_{\varepsilon/2}$ are included to eliminate terms corresponding to $\tilde{\lambda}_{ik}/N < \varepsilon/2$. The output is denoted by $|\psi_\varepsilon\rangle$, as stated formally in Lemma 5.

Lemma 5. *Given $\varepsilon > 0$, the preparation of either:*

$$|\phi_\varepsilon\rangle = \sum_{k=1}^{M_i} |u_{ik}\rangle \left| \frac{\tilde{\lambda}_{ik}}{N} \right\rangle, \quad (35)$$

or

$$|\psi_\varepsilon\rangle = \sum_{k=1}^{M_i} \sum_{l=1}^{M_j} \frac{\lambda_{ik}}{N} \langle \vec{u}_{jl}, \vec{u}_{ik} | u_{ik} \rangle |u_{jl}\rangle \left| \frac{\tilde{\lambda}_{ik}}{N} \right\rangle \left| \frac{\tilde{\lambda}_{jl}}{N} \right\rangle, \quad (36)$$

can be realized within $\tilde{O}(\frac{1}{\varepsilon})$ elementary gates and one query to U_i and U_j , where $|\tilde{\lambda}_{ik} - \lambda_{ik}| < N\varepsilon$. $M_i, M_j = O(\log N)$ is the number of kept eigenvalues of K_i, K_j after the projection $\Pi_{\varepsilon/2}$.

Denote by O_ε the quantum circuit preparing $|\psi_\varepsilon\rangle$, with which repetitive executions of phase estimation or amplitude estimation yields the value of λ_{ik} and $\lambda_{ik} |\langle \vec{u}_{jl}, \vec{u}_{ik} \rangle|$. Thus R_κ and its determinant are obtained according to Eq. 28. Selecting carefully the estimation precision and adding the preprocessing subprocedure for replacement of \mathbf{z} by $\mathbf{W}\mathbf{y}$ give the overall process estimating the contrast function with the complexity of $\tilde{O}(1/\varepsilon_1^2)$, as we stated in Theorem. 1 and 2. Their proofs are also in Appendix C.

D. Optimization

The minimization of the function with its argument being an orthogonal matrix is done by techniques for optimization on a Stiefel manifold as in [31, 33]. The remaining questions are how to utilize the difference between two theorems and whether the optimization runs successfully.

Theorem 1 allows us to first speculate the global property of $J(\mathbf{W}\mathbf{Y})$ when varying \mathbf{W} , and once $J(\mathbf{W}\mathbf{Y})$ performs like that $\mathbf{W}\mathbf{y}$ is near-independent, we can try higher accuracy without introducing much more complexity using Theorem 2 in view

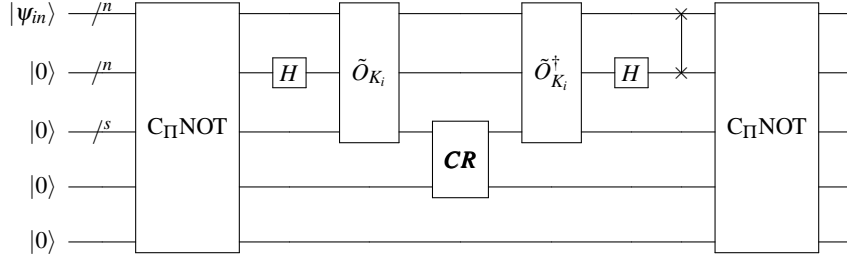


FIG. 2: The block-encoding circuit U_{K_i} of Gram matrix K_i , which outputs $\frac{K_i}{N} |\psi_{in}\rangle$ when the last $n + s + 2$ qubits are measured onto $|0^{\otimes n+s+1}, 1\rangle$. \mathbf{CR} represents the controlled rotation: $|a\rangle|0\rangle \rightarrow |a\rangle(a|0\rangle + \sqrt{1-a^2}|1\rangle)$.

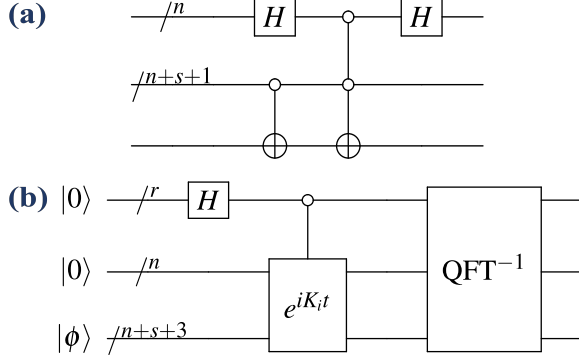


FIG. 3: (a) Schematic of the circuit of $C_{\Pi}NOT$. (b) Schematic of the eigenvalue estimation circuit U_i . The controlled $e^{iK_i t}$ represents the block encoded $e^{iK_i t}$ with t determined by r control bits. The block named QFT^{-1} is the inverse quantum Fourier transformation circuit. Measuring the first r qubits yields the estimated phases.

of the ε_2^{-1} dependence. In the near-independent case, as analyzed in Appendix D, R_κ is an identity with perturbation of magnitude ε_2 so that $J(\mathbf{W}Y) \approx 1 - \zeta \varepsilon_2$ where ζ is some constant dependent on F . Therefore the $\varepsilon_1 \varepsilon_2$ precision can always distinguish $\varepsilon_2 = a$ or $\varepsilon_2 = \frac{\zeta + \varepsilon_1}{\zeta - \varepsilon_1} a$ which allows the optimization to proceed.

Regarding the influence of the input error induced by preprocessing, we have

$$\begin{aligned} \tilde{M}^{-1/2} &= (I + (\tilde{M}^{-1/2} - M^{-1/2})M^{1/2})M^{-1/2} \\ &= (I + \varepsilon_2 E \sqrt{\|M\|_2})M^{-1/2} + o(\varepsilon_2^2) \end{aligned} \quad (37)$$

for some E with $\|E\|_2 < 1$ in the limit as ε_2 approaches 0. Using a first-order approximation with respect to ε_2 , $\tilde{M}^{-1/2}$ can be viewed as the product of matrix $M^{-1/2}$ and an orthogonal $U_E = I + \varepsilon_2 E \sqrt{\|M\|_2}$ since M is symmetric and E as well. Therefore, the optimization result only differs from the theoretically optimal solution by an orthogonal transformation, namely $\mathbf{W} = \tilde{\mathbf{W}}U_E^{-1}$. Otherwise, large ε_2 may lead to that $\tilde{M}^{-1/2}$ is not orthogonal at all and meaningless results.

The optimization is further restricted by two factors when ε_2 approaches $1/\sqrt{N}$. One is that the statistical error plays an important role since the samples are in general not perfect and the other is the higher demand for the accuracy for distinguishability.

IV. NUMERICAL EXPERIMENTS

We present numerical tests for assessment of the capability of our algorithm to separate the ICs and to support Theorem 1. In the first half, the raw data is sampled by the given PDF, as illustrated in Fig. 5, and a biological dataset is used later to introduce examples of applications.

In the first stage, data sampled from a given PDF are seen as samples of an IC s_i . After a linear transformation \mathbf{A} , mixtures $\mathbf{A}S$ are sent for computing the contrast function so that it is convenient to observe its performance as \mathbf{A} varies. Fig. 6a reveals the performance of the contrast function used in the original KICA algorithm, while Fig. 6b, 6c and 6d illustrate cases using the adapted one with measuring error, $\varepsilon_1 = 0, 2, 4 \times 10^{-3}$, respectively. Contrast functions can always approach their minima in our test. We find the adaptation of the contrast function does not appear to destroy the effectiveness after comparing these results.

Vary sample size and mixing coefficients at the same time, then we compute norms of states of $|K_i\rangle$ and $|\psi_\varepsilon\rangle$, results given in Fig. 7a and 7b. This reveals that only the extent of mixing is dominant for the success rate problem, and the probability problem occurs mainly when the mixture tends to be unmixed.

The relation between $\|\psi_\varepsilon\rangle\|$ and sample size N is further shown in Fig. 8a. We set mixing coefficients to be $\exp\{i\delta P\}$, a fixed δ for each curve. It is found that in double logarithmic coordinates, the slope of each curve increases gradually from 1/2 to 1 as N goes up except in the case that $\delta = 0$, where the slope stays at 1/2. Our fitted curves agree with our expectation that $\|\psi_\varepsilon\rangle\| = O(\varepsilon_2 + 1/\sqrt{N})$, while in this case ε_2 can be identified with δ .

Fix the mixing coefficients to $\exp\{i(0.1\pi P)\}$, we illustrate the relation between the error of $\det(R_\kappa)$ and ε_1 as N increases in Fig. 8b. Because of the significant effect of randomness, the fit has a certain variance but it is enough to show the error increases linearly with ε_1 but hardly with N .

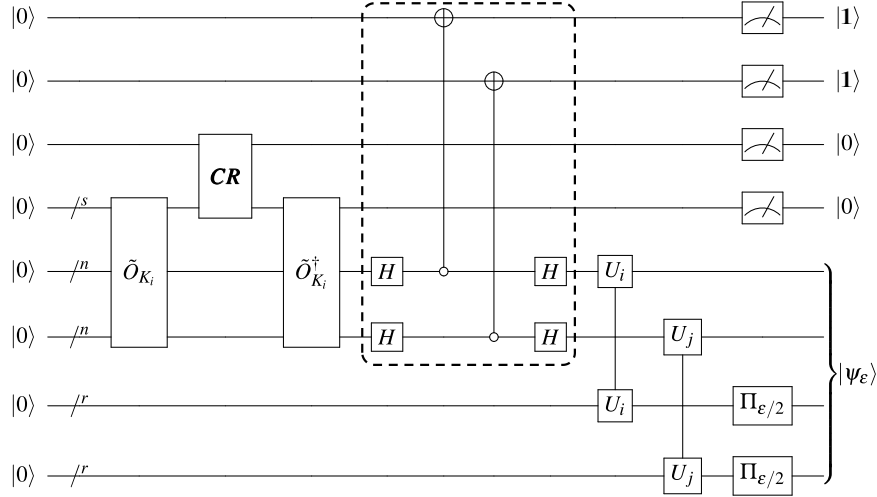


FIG. 4: Schematic of the circuit that prepares state $|\psi_\epsilon\rangle$, where \tilde{O}_{K_i} is the block encoding of K_i and U_i is the eigenvalue estimation circuit. Gates enclosed by the dashed line are used for an amplitude encoding of K_i from one of \tilde{K}_i .

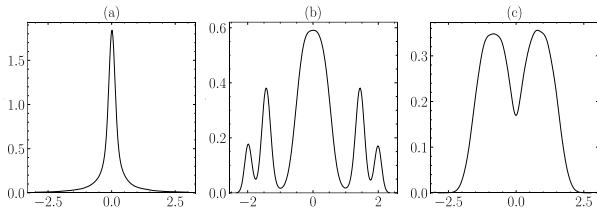


FIG. 5: Probability density functions of partial ICs.

With the same setup where δ_1 and δ_2 are variable, the minimum eigenvalues ξ of R_κ are given in Fig. 9a. We also repeat randomly choosing mixing coefficients for ξ and select the minimal for each fixed sample size. Each data point in Fig. 9b represents the lowest ξ we have met during our test for corresponding N , where no apparent numerical relationship appears even in such large ranges. Our upper bound of the error of $J(X)$ seems not to fail in more general cases.

Finally, we classically simulate the optimizer together with our contrast function computation subprogram. With the ICs shown in Fig. 5, we recorded the optimized unmixing coefficient matrices which are then assessed by a metric named "Amari error" [31, 37]. If the known mixing coefficients matrix is \mathbf{A} , while the optimized unmixing matrix reads \mathbf{W}^{-1} , the Amari error is defined by

$$\epsilon_A(\mathbf{A}, \mathbf{W}) = \frac{1}{2m} \sum_{i=1}^m \left(\frac{\sum_{j=1}^m |a_{ij}|}{\max_j |a_{ij}|} - 1 \right) + \frac{1}{2m} \sum_{j=1}^m \left(\frac{\sum_{i=1}^m |a_{ij}|}{\max_i |a_{ij}|} - 1 \right), \quad (38)$$

where $a_{ij} = (\mathbf{A}\mathbf{W}^{-1})_{ij}$. Fig. 10 shows that ϵ_A decreases with

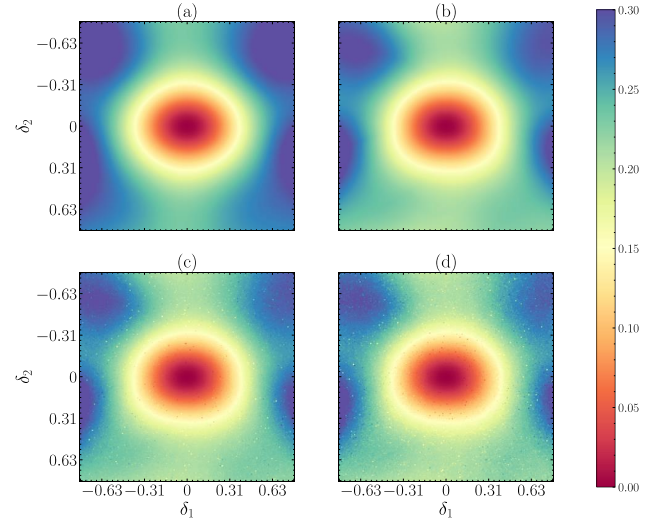


FIG. 6: Values of $-\ln(\det(R_\kappa))$ represented by colors when varying the mixing coefficients, $\exp\{i(\delta_1 P_1 + \delta_2 P_2)\}$. P_1, P_2 are two generators, and δ_1, δ_2 are parameters reflecting the deviation of the mixtures from the original ICs. (a) $-\ln(\det(R_\kappa))$ computed with the correct signs of $\langle \vec{u}_{ik}, \vec{u}_{jl} \rangle$; (b), (c), (d) $-\ln \det(R_\kappa)$ computed with measuring error $\epsilon_1 = 0, 2, 4 \times 10^{-3}$ respectively, signs of entries of R_κ neglected.

N , which is intuitive for a feasible ICA algorithm.

To illustrate an example of applications, we introduce a transcriptomic dataset [12]. It contains the expression of

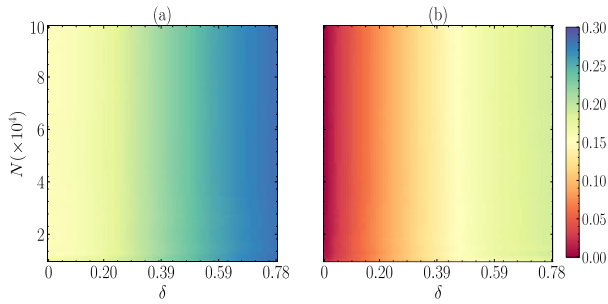


FIG. 7: Represented by colors, norms of different quantum states computed with mixing coefficients $\exp\{i\delta P\}$ as N and δ increase. (a) Norms of $|K_i\rangle$; (b) Norms of $|\psi_\epsilon\rangle$.

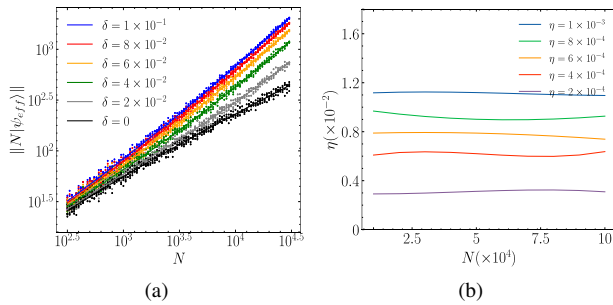


FIG. 8: (a) The norm of $|\psi_\epsilon\rangle$ computed with mixing coefficients $\exp\{i\delta P\}$ as sample size N and δ vary and P is one of the generators. (b) Relative error of $\det(R_\kappa)$, $\eta = |(\det(R_\kappa) - \det(\tilde{R}_\kappa)) / \det(R_\kappa)|$, as a function of N when introducing measuring error to be ϵ .

genes for patients with lung cancer. We simulate our algorithm to separate the latent ICs from this dataset with a simplified optimization process. Compare our results of decomposition with the one obtained by stabilized-ica (sica) package based on Icasto algorithm [38], available from <https://github.com/ncaptier/stabilized-ica>. The correlation matrix between ICs separated in different ways is shown in Fig. 10b. A clear correlation exists between two sets of ICs.

V. CONCLUSION

In this paper, we have presented a quantum ICA algorithm scaling as $\tilde{O}(1/\epsilon_1^2)$ to estimate a contrast function adapted from the one of classical KICA algorithm with the precision of ϵ_1 . Our method exponentially accelerates the computation of KICA. This speedup comes from the better performance of matrix operations offered by quantum arithmetics, QSVT, amplitude estimation, etc. We have provided an upper bound of the error of the estimated R_κ which gives the scaling of the error of the contrast function. This verifies that the exponential speedup is generally achievable. Compared to the existing quantum algorithms for ICA based upon kurtosis or entropy,

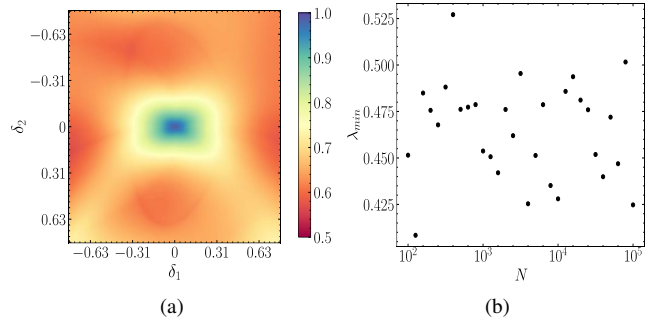


FIG. 9: (a) The minimal eigenvalues of R_κ for various mixtures, $\exp\{i(\delta_1 P_1 + \delta_2 P_2)\}S$, where S are given ICs. (b) For fixed sample size, each datapoint represents the lowest one among all the minimal eigenvalues of $R_\kappa(\mathbf{W}S)$ for randomly selected mixing coefficients \mathbf{W} .

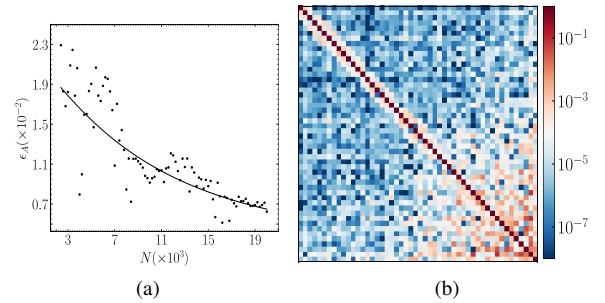


FIG. 10: (a) Amari error ϵ_A between the optimized mixing coefficients and the pre-known one as N increases. (b) Correlation matrix between ICs computed by classically simulating our algorithm and by the Icasto algorithm called from the stabilized-ica package. The color of the grid in row i , column j corresponds to the correlation coefficient between the i -th and the j -th ICs separated with each method.

our method seems to be a compromise between robustness and efficiency.

In Appendix D, we asymptotically analyze why the Gaussian kernel is an appropriate choice for the KICA algorithm by research of $R_\kappa(Z)$, whose off-diagonal elements cannot be all zero unless all the random variables z_i are mutually independent if Gaussian kernel is chosen and z_i are near-independent. It will occur that the contrast function decreases from the center to the periphery when Z is taken among different perturbations of independent components regardless of the statistical error.

We implemented numerical experiments with raw data sampled from given distributions and a biomedical dataset. These samples were then sent for estimation of contrast function, success rate, error performance, the effectiveness of separation, etc. to ensure the reliability and further reveal the performance of our adapted algorithm. The error and the success rate were also checked to be consistent with our analysis.

However, we have not yet considered whether such dis-

tributions exist that $R_{\kappa}(Z) = I$ but \mathbf{z}_i are not mutually independent at all. If they exist, the performance around this extremum is left for further consideration.

It is seen that we perform a principal components analysis of $K_i^T K_i$ which may be worse than directly analyzing K_i which might be realized by the block-encoding technique introduced in [39]. Moreover, perhaps the input model can be replaced by $O_{f_{x_i}} : |0\rangle \rightarrow \sum_x \sqrt{f_{x_i}(x)} |x\rangle$, for PDF of x_i, f_{x_i} . Such input model gives the possibility to estimate statistical properties with the precision of ε using $O(\varepsilon^{-1})$ queries [30, 40], compared to $O(\varepsilon^{-2})$ sampling complexity in classical cases. It is also possible that the model similarly reduces the sampling complexity when computing the contrast function.

ACKNOWLEDGMENTS

This work was supported by the National Natural Science Foundation of China (Grant No. 12034018) and Innovation Program for Quantum Science and Technology (Grant No. 2021ZD0302300).

The numerical calculations in this paper have been done on the supercomputing system in the Supercomputing Center of University of Science and Technology of China.

Appendix A: ICA based on statistics and quantum speedup

Non-Gaussianity has been widely used as a measure of the independence in some ICA models. Such as kurtosis or mutual information, statistics can naturally represent the non-Gaussianity [27]. As introduced later, existing quantum algorithms have shown advantages in estimating these statistics.

For simplicity, we assume components \mathbf{y}_i of the random vector \mathbf{y} have been whitened. And quantum oracles O_{y_i} are given. We introduce the two measures of non-Gaussianity and their estimation on a quantum computer in this section. The corresponding optimization is similar to what we have introduced in our algorithm.

1. ICA based upon kurtosis

The kurtosis of \mathbf{y}_i is defined by

$$\text{kurt}(\mathbf{y}_i) = E\{\mathbf{y}_i^4\} - 3(E\{\mathbf{y}_i^2\})^2. \quad (\text{A1})$$

Suppose each IC \mathbf{s}_i has kurtosis with the same sign. It is proved that the mixture, $\mathbf{a}^T \mathbf{y}$ where $\|\mathbf{a}\|_2 = 1$, has the maximal absolute kurtosis when $\mathbf{a}^T \mathbf{y}$ is properly one of the ICs[41]. Therefore, optimizing $|\text{kurt}(\mathbf{a}^T \mathbf{y})|$ gives one of the ICs.

The quantum mean estimator introduced can achieve the estimation, just by estimating using the oracle $O_{y_i^k} : |j\rangle|0\rangle \rightarrow |j\rangle|y_{ij}^k\rangle$ constructed by quantum arithmetics. The query and gate complexity is $\tilde{O}(1/\varepsilon)$, for ε being the estimation precision. It is worth noting that this methodology can be applied to other ICA algorithms using mean estimators such as the notable FastICA algorithm [15].

2. ICA based upon mutual information

Mutual information is a strong candidate as a choice of contrast function, which can be defined by Shannon's entropy. The Shannon entropy of \mathbf{y} is

$$H(\mathbf{y}) = - \int f_{\mathbf{y}}(\boldsymbol{\alpha}) \log f_{\mathbf{y}}(\boldsymbol{\alpha}) d\boldsymbol{\alpha}, \quad (\text{A2})$$

where $f_{\mathbf{y}}$ is the PDF of \mathbf{y} . It reads

$$H(\mathbf{y}) = - \sum_{\boldsymbol{\gamma}} p_{\boldsymbol{\gamma}} \log p_{\boldsymbol{\gamma}}, \quad (\text{A3})$$

for a discrete one, where $p_{\boldsymbol{\gamma}}$ is the probability that $\mathbf{y}_i = \gamma_i, i = 1, 2, \dots, m$. Then the mutual information I between \mathbf{y}_i is given by

$$I(\mathbf{y}) \equiv I(\mathbf{y}_1, \mathbf{y}_2, \dots, \mathbf{y}_m) = \sum_{i=1}^m H(\mathbf{y}_i) - H(\mathbf{y}). \quad (\text{A4})$$

It is nonnegative, and zero if and only if \mathbf{y} are mutually independent, and therefore a natural measure of the independence.

A quantum Shannon's entropy estimator exists, as introduced in [42], with both query and gate complexity of $\tilde{O}(\frac{\sqrt{N}}{\varepsilon^2})$. For comparison, $\tilde{O}(1/\varepsilon)$ queries suffices to estimate $E\{\mathbf{y}_i^p\}$ or $\text{kurt}(\mathbf{y}_i)$ and $\tilde{O}(1/\varepsilon^2)$ queries are required for the adapted KICA contrast function. The kurtosis is known to be not robust so our adapted one may serve as a compromise between efficiency and robustness.

Appendix B: Error analysis

We refer to \tilde{a} as an estimate of some variable a in this section.

1. The error of preprocessing

We first analyze the error of the constructed O_{y_i} in Eq. 22. We denote the covariance matrix of \mathbf{x} by M , and we have

$$\begin{aligned} |\tilde{M}_{ij} - M_{ij}| &\leq |\tilde{E}\{\mathbf{x}_i \mathbf{x}_j\} - \tilde{E}\{\mathbf{x}_i \mathbf{x}_j\}| + \\ &|\tilde{E}\{\mathbf{x}_i\} \tilde{E}\{\mathbf{x}_j\} - E\{\mathbf{x}_i\} E\{\mathbf{x}_j\}| < \frac{1}{2} \frac{\|M\|_2^{3/2} \varepsilon}{\mu_M^2 m} \end{aligned} \quad (\text{B1})$$

Next, we estimate the error of the inverse of the covariance matrix M^{-1} , where we denote $D \equiv \tilde{M} - M$:

$$\frac{\|M^{-1} - \tilde{M}^{-1}\|_2}{\|M^{-1}\|_2} \leq \frac{\|M^{-1} D\|_2}{1 - \|M^{-1} D\|_2}. \quad (\text{B2})$$

Eq. B2 works only if $\|M^{-1} D\|_2 \leq 1$. Note that

$$\|M^{-1} D\|_2 \leq \frac{\mu_M}{\|M\|_2} \times m \times \frac{1}{2} \varepsilon \frac{\|M\|_2^{3/2}}{\mu_M^2 m} = \frac{1}{2} \frac{\varepsilon \sqrt{\|M\|_2}}{\mu_M} < 1. \quad (\text{B3})$$

The first inequality comes from that $\|D\|_2 \leq \|D\|_F \leq m \times \max_{i,j}\{D_{ij}\}$. Now we may apply the inequality and have,

$$\|\tilde{M}^{-1} - M^{-1}\|_2 \leq \frac{\frac{1}{2}\|M\|_2^{-1/2}\varepsilon}{1 - \frac{1}{2}\frac{\varepsilon\sqrt{\|M\|_2}}{\mu_M}}. \quad (\text{B4})$$

Introduce a theorem for further estimation.

Theorem 3. [43] For two positive definite matrix A, B , if eigenvalues of A, B are bounded below some by positive number a , thus we have the inequality

$$\| |A^r - B^r| \| \leq ra^{r-1} \| |A - B| \|, \quad 0 < r < 1, \quad (\text{B5})$$

where $\| |\cdot| \|$ refers to a unitarily invariant norm including 2-norm we used later.

The maximal eigenvalue of \tilde{M} is bounded above by $\|M\|_2 + \|D\|_2 < \|M\|_2 + \varepsilon \frac{\|M\|_2^{3/2}}{2\mu_M^2}$. Replace A, B, a, r in Theorem 3 by $M^{-1}, \tilde{M}^{-1}, (\|M\|_2 + \varepsilon \frac{\|M\|_2^{3/2}}{2\mu_M^2})^{-1}, \frac{1}{2}$, we have:

$$\begin{aligned} & \|\tilde{M}^{-\frac{1}{2}} - M^{-\frac{1}{2}}\|_2 \\ & < \frac{1}{2} (\|M\|_2 + \varepsilon \frac{\sqrt{\|M\|_2}}{2\mu_M^2})^{\frac{1}{2}} \frac{\frac{1}{2}\|M\|_2^{-1/2}\varepsilon}{1 - \frac{1}{2}\frac{\varepsilon\sqrt{\|M\|_2}}{\mu_M}} \\ & < \frac{1}{2} \sqrt{\frac{3}{2}} \sqrt{\|M\|_2} \times \|M\|_2^{-1/2} \varepsilon < \varepsilon. \end{aligned} \quad (\text{B6})$$

2. The error of entries of R_κ

In this section, the error bound of $\frac{\lambda_{ik}}{\lambda_{ik} + N\kappa/2} \frac{\lambda_{jl}}{\lambda_{jl} + N\kappa/2} \langle \vec{u}_{ik}, \vec{u}_{jl} \rangle$ in cases of Theorem 1 and 2 is proved.

Use notations that ε_μ and ε_I represent respectively the error of μ_{ik} induced by phase estimation and of $\mu_{ik} \langle \vec{u}_{ik}, \vec{u}_{jl} \rangle$ induced by amplitude estimation for simplicity. Only entries with either μ_{ik} or $\mu_{jl} < \varepsilon_\mu$ may be discarded. The discarded entry where $\mu_{ik} < \varepsilon_\mu$ reads

$$\frac{\mu_{ik}}{\mu_{ik} + \kappa/2} \frac{\mu_{jl}}{\mu_{jl} + \kappa/2} \langle \vec{u}_{ik}, \vec{u}_{jl} \rangle < \frac{\varepsilon_\mu}{\varepsilon_\mu + \kappa/2} \times 1 < \frac{\xi \varepsilon_1}{2}, \quad (\text{B7})$$

for the first case, and

$$\frac{\mu_{ik}}{\mu_{ik} + \kappa/2} \frac{\mu_{jl}}{\mu_{jl} + \kappa/2} \langle \vec{u}_{ik}, \vec{u}_{jl} \rangle < \frac{2}{\kappa} \varepsilon_\mu \times G \varepsilon_2 = \frac{\varepsilon_1 \varepsilon_2}{2}, \quad (\text{B8})$$

for the second, while this analysis also works when $\mu_{jl} < \varepsilon_\mu$. For entries kept, the following results can be then computed:

$$\left| \frac{\mu_{ik}}{\mu_{ik} + \kappa/2} - \frac{\tilde{\mu}_{ik}}{\tilde{\mu}_{ik} + \kappa/2} \right| < \frac{\kappa/2}{\tilde{\mu}_{ik} + \kappa/2} \frac{\varepsilon_\mu}{\mu_{ik} + \kappa/2}, \quad (\text{B9})$$

$$\left| \frac{1}{\mu_{ik} + \kappa/2} - \frac{1}{\tilde{\mu}_{ik} + \kappa/2} \right| < \frac{1}{\tilde{\mu}_{ik} + \kappa/2} \frac{\varepsilon_\mu}{\mu_{ik} + \kappa/2}. \quad (\text{B10})$$

Combining these two errors and ε_I , we give the error bound of entries by:

$$\begin{aligned} & \frac{\kappa/2}{\tilde{\mu}_{jl} + \kappa/2} \frac{\varepsilon_\mu}{\mu_{jl} + \kappa/2} \frac{\mu_{ik} \langle \vec{u}_{ik}, \vec{u}_{jl} \rangle}{\mu_{ik} + \kappa/2} + \\ & \frac{\tilde{\mu}_{jl} \mu_{ik} \langle \vec{u}_{ik}, \vec{u}_{jl} \rangle}{\tilde{\mu}_{jl} + \kappa/2} \frac{1}{\tilde{\mu}_{ik} + \kappa/2} \frac{\varepsilon_\mu}{\mu_{ik} + \kappa/2} + \varepsilon_I \frac{\tilde{\mu}_{jl}}{\tilde{\mu}_{jl} + \kappa/2} \frac{1}{\tilde{\mu}_{ik} + \kappa/2} \\ & < \frac{\varepsilon_\mu \mu_{ik}}{\tilde{\mu}_{jl} + \kappa/2} \frac{\langle \vec{u}_{ik}, \vec{u}_{jl} \rangle}{\mu_{ik} + \kappa/2} \left(\frac{2}{\kappa} \tilde{\mu}_{jl} + 1 \right) + \varepsilon_I \frac{1}{\tilde{\mu}_{ik} + \kappa/2} \frac{\tilde{\mu}_{jl}}{\tilde{\mu}_{jl} + \kappa/2} \\ & < \frac{2}{\kappa} \varepsilon_\mu \langle \vec{u}_{ik}, \vec{u}_{jl} \rangle + \frac{2}{\kappa} \varepsilon_I. \end{aligned} \quad (\text{B11})$$

It is evident that for the two cases, we have, respectively,

$$\frac{2}{\kappa} \varepsilon_\mu \langle \vec{u}_{ik}, \vec{u}_{jl} \rangle + \frac{2}{\kappa} \varepsilon_I \leq \xi \varepsilon_1, \quad (\text{B12})$$

and

$$\frac{2}{\kappa} \varepsilon_\mu \langle \vec{u}_{ik}, \vec{u}_{jl} \rangle + \frac{2}{\kappa} \varepsilon_I \leq \varepsilon_1 \varepsilon_2. \quad (\text{B13})$$

To summarize, the expected error bound of R_κ entries has been proved.

3. The error of $J(Z)$

Now we estimate the error of $\det(R_\kappa)$, when additive error of entries of R_κ is bounded by ε , we have $\|\tilde{R}_\kappa - R_\kappa\|_2 \leq \varepsilon d$ where d is the dimension of R_κ . According to the inequality [44]: Let A and B be $d \times d$ matrices, thus it holds that

$$\left| \frac{\det(A+B) - \det(A)}{\det(A)} \right| \leq \frac{d\mu_A \|B\|/\|A\|}{1 - d\mu_A \|B\|/\|A\|}, \quad (\text{B14})$$

when $d\mu_A \|B\|/\|A\| \leq 1$, where μ_A is the condition number of A . To apply this inequality, it requires that $d^2 \varepsilon \mu_{R_\kappa} / \|R_\kappa\|_2 \leq 1$, where $d = \Theta(m \log N)$ and $\|R_\kappa\|_2 / \mu_{R_\kappa}$ is exactly ξ . It suffices to choose $\varepsilon < \frac{\xi}{2d^2}$. Substitute $A = R_\kappa$ and $B = R_\kappa - \tilde{R}_\kappa$ into Eq. B14, we have

$$\left| \frac{\det(\tilde{R}_\kappa) - \det(R_\kappa)}{\det(R_\kappa)} \right| \leq \frac{d^2 \varepsilon \xi^{-1}}{1 - d^2 \varepsilon \xi^{-1}}. \quad (\text{B15})$$

Then relative error $\eta = |(\det(\tilde{R}_\kappa) - \det(R_\kappa)) / \det(R_\kappa)|$ scales as $O(\xi^{-1} \varepsilon m^2 \log^2 N)$.

Appendix C: Proofs of conclusions

1. Proof of Lemma 2

We provide the effect of the circuit as proof. $O_{z_i} \otimes O_{z_i}$ implemented on the initial state $|i\rangle|0\rangle \otimes |j\rangle|0\rangle$ gives

$$(O_{z_i} \otimes O_{z_i}) |j\rangle|0\rangle \otimes |k\rangle|0\rangle = |j\rangle|z_{ij}\rangle \otimes |k\rangle|z_{ik}\rangle. \quad (\text{C1})$$

Next estimate kernel function in Eq. 9 by quantum arithmetics on a newly introduced quantum register initialized to $|z\rangle$ with $s = \lceil \log_2(1/\varepsilon) \rceil$ qubits:

$$|j\rangle|z_{ij}\rangle|k\rangle|z_{ik}\rangle|z\rangle \rightarrow |j\rangle|z_{ij}\rangle|k\rangle|z_{ik}\rangle|z \oplus K(z_{ij}, z_{ik})\rangle. \quad (\text{C2})$$

Uncompute z_{ij} and z_{ik} by $O_{z_i}^\dagger$:

$$|j\rangle|0\rangle|k\rangle|0\rangle|z \oplus K(z_{ij}, z_{ik})\rangle, \quad (\text{C3})$$

which achieves the goal of the lemma. Overall quantum arithmetics cost no more than $O(\text{polylog}(N/\varepsilon))$ quantum gates, and 2 queries to O_{z_i} and $O_{z_i}^\dagger$, with precision of $K(z_{ij}, z_{ik})$ up to ε .

2. Proof of Lemma 3

First, we have

$$\begin{aligned} & (I_{2n} \otimes \mathbf{CR})(\tilde{O}_{K_i} \otimes I_1)(I_n \otimes H^{\otimes n} \otimes I_{s+1})|j\rangle|0^{\otimes s+1}\rangle \\ &= \frac{1}{\sqrt{N}} \sum_{r=1}^N |j\rangle|r\rangle \left(|(\tilde{K}_i)_{jr}\rangle \langle (\tilde{K}_i)_{jr}|0\rangle + \sqrt{1 - (\tilde{K}_i)_{jr}^2} |1\rangle \right), \end{aligned} \quad (\text{C4})$$

and

$$\begin{aligned} & (\mathbf{SWAP}_n \otimes I_{s+1})(\tilde{O}_{K_i} \otimes I_1)(I_n \otimes H^{\otimes n} \otimes I_{s+1})|k\rangle|0^{\otimes s+1}\rangle \\ &= \frac{1}{\sqrt{N}} \sum_{t=1}^N |t\rangle|k\rangle|0^{\otimes s+1}\rangle. \end{aligned} \quad (\text{C5})$$

Combining the two gives that

$$\langle k|\langle 0^{\otimes n+s+1}|\tilde{U}_{K_i}|j\rangle|0^{\otimes n+s+1}\rangle = \frac{(\tilde{K}_i)_{jk}}{N} = \frac{(\tilde{K}_i)_{kj}}{N}. \quad (\text{C6})$$

The controlled rotation can be implemented with the complexity of $O(\text{polylog}(N/\varepsilon))$ for the precision of rotation up to ε . Therefore, an $(N, n+s+1, \varepsilon)$ -block-encoding of \tilde{K}_i is given, which uses $O(\text{polylog}(N/\varepsilon))$ elementary gates and one query to \tilde{O}_{K_i} and its inverse, as discussed in [36]. For our purpose, introduce another ancilla and then $C_{\Pi} \text{NOT} \cdot \tilde{U}_{K_i} \cdot C_{\Pi} \text{NOT}$ is an $(N, n+s+2, \varepsilon)$ -block-encoding of K_i/N , since with the projection,

$$\Pi = (I_n - |\vec{1}\rangle\langle \vec{1}|) \otimes |0^{\otimes n+s+1}\rangle\langle 0^{\otimes n+s+1}|. \quad (\text{C7})$$

we have

$$\Pi \tilde{U}_{K_i} \Pi = \frac{K_i}{N} \otimes |0^{\otimes n+s+1}\rangle\langle 0^{\otimes n+s+1}|, \quad (\text{C8})$$

where we use the relation that $K_i = (I_n - |\vec{1}\rangle\langle \vec{1}|)\tilde{K}_i(I_n - |\vec{1}\rangle\langle \vec{1}|)$.

3. Proof of Lemma 4

Ignore the error induced by block-encoding process because of the $\text{polylog}(N/\varepsilon)$ dependence, the block-encoding

of the $e^{iK_i t}$ also has the eigenvalue $e^{i\lambda_{ik} t}$ for eigenvector $|u_{ik}\rangle$, in the subspace where the last $n+s+2$ qubits are set $|0^{\otimes n+s+1}, 1\rangle$. Therefore, the effect of the phase estimation of $e^{iK_i t}$ is as claimed for U_i . The complexity comes mainly from the phase estimation, scaling as $\tilde{O}(1/\varepsilon)$ for both query and gate one.

4. Proof of Lemma 5

The quantum circuit illustrated in Fig. 4 accomplishes the state preparation. We have, for the first part,

$$\begin{aligned} & (\mathbf{CR} \otimes I_{2n})(I \otimes \tilde{O}_{K_i})|0^{\otimes 1+s}, 0^{\otimes s+2n}\rangle = \\ & \sum_{j,k=1}^N (\tilde{K}_i)_{jk} |0^{\otimes 1+s}, j, k\rangle + |\perp_1\rangle. \end{aligned} \quad (\text{C9})$$

The second part is a projection so that

$$\sum_{j,k=1}^N (\tilde{K}_i)_{jk} |0^{\otimes 2}, j, k\rangle \rightarrow \sum_{j,k=1}^N (K_i)_{jk} |1^{\otimes 2}, j, k\rangle + |\perp_2\rangle. \quad (\text{C10})$$

Represent $|K_i\rangle$ in the basis of eigenvectors of K_i by

$$|K_i\rangle = \frac{1}{N} \sum_{k=1}^N \lambda_{ik} |u_{ik}\rangle |u_{ik}\rangle. \quad (\text{C11})$$

Use the superscript to label the register, Eq. 35 comes up by

$$\begin{aligned} |\phi_\varepsilon\rangle &= \Pi_{\varepsilon/2}^3 U_i^{13} |K_i\rangle_{12} |0\rangle_3 |0\rangle_4 = \\ & \sum_{k=1}^N \frac{\lambda_{ik}}{N} |u_{ik}\rangle_1 |u_{ik}\rangle_2 \frac{\tilde{\lambda}_{ik}}{N} |0\rangle_3 |0\rangle_4. \end{aligned} \quad (\text{C12})$$

then the output of the quantum circuit in Fig. 4 is written by

$$\begin{aligned} |\psi_\varepsilon\rangle &= \Pi_{\varepsilon/2}^4 \Pi_{\varepsilon/2}^3 U_j^{24} U_i^{13} |K_i\rangle_{12} |0\rangle_3 |0\rangle_4 = \\ & \sum_{k,l=1}^N \frac{\lambda_{ik}}{N} \langle u_{jl} | u_{ik} \rangle |u_{ik}\rangle_1 |u_{jl}\rangle_2 \frac{\tilde{\lambda}_{ik}}{N} |0\rangle_3 \frac{\tilde{\lambda}_{jl}}{N} |0\rangle_4. \end{aligned} \quad (\text{C13})$$

Let the precision of phase estimation be $\varepsilon/2$, and we have the claimed precision since eigenvalues larger than ε would not be discarded. The complexity of the preparation comes mainly from U_i, U_j , scaling as $\tilde{O}(\frac{1}{\varepsilon})$, which completes the proof.

5. Proof of Theorem 1

Note that K_i is the same for \tilde{y}_{ij} respectively in Eqs. 16 and 23, so the distinction does not matter. Substitute $\mathbf{z} = \tilde{\mathbf{y}}'$ for Lemma 5. Let $\varepsilon = \frac{\xi \kappa \varepsilon_1}{4}$ for O_ε . Implement the amplitude estimation of O_ε with precision of also $\frac{\xi \kappa \varepsilon_1}{4}$. Directly compute $R_\kappa(\mathbf{Z})$ and $J(\mathbf{Z})$ with estimated λ_{ik} and $\lambda_{ik} |\langle u_{jl} | u_{ik} \rangle|$. As shown in Appendix B 2 and B 3, such estimation has the multiplicative error bounded above by $2d^2 \varepsilon_1$. Combined with the error induced by preprocessing in Lemma 1 with the precision of ε_2 , where it suffices to estimate the covariance matrix just once, here we accomplish the proof.

6. Proof of Theorem 2

Also do the substitution $\mathbf{z} = \tilde{\mathbf{y}}'$. Given an upper bound of $|\langle \tilde{\mathbf{u}}_{jl}, \tilde{\mathbf{u}}_{ik} \rangle|$ for arbitrary i, k, j, l by $\varepsilon_2 G$. G is asymptotically a constant irrelevant to $N, \varepsilon_1, \varepsilon_2$ as in Appendix D. Let $\varepsilon = \frac{\kappa \varepsilon_1}{4G}$. Implement the amplitude estimation of O_ε with precision of $\frac{\varepsilon_1 \varepsilon_2 \kappa}{4}$. Note that the minimal eigenvalue ξ of $R_\kappa(Z)$ is bounded below by $1 - d\varepsilon_2 G$. Using results in Appendix B 2 and B 3 proves that the directly computed $J(Z)$ has multiplicative error bounded above by $O(d^2 \varepsilon_1 \varepsilon_2)$. Further consideration of preprocessing with the precision of ε_2 completes the proof.

7. Proof of Lemma 6

Due to the factor $(\hat{I} - \hat{I}_i)$ of \hat{K} , we have

$$\hat{I}_i \phi_{ik} = \int_{\mathbb{R}} \phi_{ik}(x) f_{z_i}(x) dx = 0. \quad (\text{C14})$$

Up to the first order terms of ε , we have first $F_{ij} = F_{ji} + O(\varepsilon^2)$. The joint distribution of z_i, z_j can be written as

$$f_{z_i, z_j}(x, y) = f_{z_i}(x) f_{z_j}(y) - \varepsilon \alpha_{ij} \left(y \frac{\partial}{\partial x} - x \frac{\partial}{\partial y} \right) f_{s_i}(x) f_{s_j}(y) + O(\varepsilon^2). \quad (\text{C15})$$

The distribution of z_i is almost invariant, namely $f_{x_i}(x) = f_{s_i}(x) + O(\varepsilon^2)$. Considering Eq.C14, we have

$$\begin{aligned} M_{z_i, z_j}(\phi_{ik}, \phi_{jl}) &= \int_{\mathbb{R}^2} \phi_{ik}(x) \phi_{jl}(y) [f_{z_i}(x) f_{z_j}(y) - \\ &\varepsilon \alpha_{ij} \left(y \frac{\partial}{\partial x} - x \frac{\partial}{\partial y} \right) f_{s_i}(x) f_{s_j}(y) + O(\varepsilon^2)] dx dy \\ &= \varepsilon \alpha_{ij} \int_{\mathbb{R}^2} \phi_{ik}(x) \phi_{jl}(y) \left(x \frac{\partial}{\partial y} - y \frac{\partial}{\partial x} \right) f_{s_i}(x) f_{s_j}(y) dx dy + O(\varepsilon^2). \end{aligned} \quad (\text{C16})$$

8. Proof of Lemma 7

That

$$\int_{\mathbb{R}^2} d\rho_{s_i}(x) d\rho_{s_j}(y) \left(x \frac{\partial}{\partial y} - y \frac{\partial}{\partial x} \right) \phi_{ik}(x) \phi_{jl}(y) \quad (\text{C17})$$

is always 0 for all k, l such that $\mu_{ik}, \mu_{jl} \neq 0$ is equivalent to

$$\int_{\mathbb{R}^2} d\rho_{s_i}(x) d\rho_{s_j}(y) \left(x \frac{\partial}{\partial y} - y \frac{\partial}{\partial x} \right) K'_i(x, \alpha) K'_j(y, \beta) = 0. \quad (\text{C18})$$

Use the following notation:

$$g_i(\alpha) = \int_{\mathbb{R}} d\rho_{s_i}(x) K(x, \alpha), \quad (\text{C19})$$

$$g'_i(\alpha) = \int_{\mathbb{R}} d\rho_{s_i}(x) \frac{\partial}{\partial x} K(x, \alpha), \quad (\text{C20})$$

$$C_i = \int_{\mathbb{R}} d\rho_{s_i}(\alpha) \alpha g_i(\alpha), \quad (\text{C21})$$

similarly for the definition of g_j, C_j . Omitting the terms that are 0 after integration or differential and substituting expression of Gaussian kernel (where we take $\sigma = 1/\sqrt{2}$ for simplicity, little difference for other values of σ), Eq.C18 is then

$$\begin{aligned} 2\beta g_j(\beta) [\alpha g_i(\alpha) - \frac{1}{2} g'_i(\alpha)] - C_i g'_j(\beta) - \\ 2\alpha g_i(\alpha) [\beta g_j(\beta) - \frac{1}{2} g'_j(\beta)] + C_j g'_i(\alpha) = 0. \end{aligned} \quad (\text{C22})$$

The above equation is simplified to

$$[C_i - \beta g_j(\beta)] g'_i(\alpha) = [C_j - \alpha g_i(\alpha)] g'_j(\beta), \quad (\text{C23})$$

which leads to three solutions:

$$(1), g_i(\alpha) = C_j / \alpha \quad (\text{C24})$$

$$(2), g'_i(\alpha) = g'_j(\beta) = 0, \quad (\text{C25})$$

$$(3), g'_i(\alpha) + k[C_j - \alpha g_i(\alpha)] = 0 \rightarrow \\ g_i(\alpha) = e^{-a_1 \alpha^2} (a_2 + a_3 \int_0^\alpha e^{a_1 \alpha'^2} d\alpha'). \quad (\text{C26})$$

Conditions that $\int_{\mathbb{R}} f_{s_i}(x) dx = 1$, $f_{s_i}(x) > 0$ and $K(x, \alpha) = \exp\{-(x - \alpha)^2\}$ requires $\lim_{\alpha \rightarrow \infty} g_i(\alpha) = 0$ so that the first two solutions should be discarded and $a_3 = 0$ for the last solution. $g_i(\alpha) = a_2 e^{-a_1 \alpha^2}$ leads to that f_{s_i} must have the form of $\frac{\exp\{-x^2/\sigma_i^2\}}{\sqrt{2\pi\sigma_i}}$, i.e. \mathbf{s}_i is Gaussian. The discussion above also works for \mathbf{s}_j which completes the proof.

Appendix D: Asymptotic properties

In this section, we analyze the asymptotic properties of $K_i(Z)$ when \mathbf{z} can be written as

$$\mathbf{z} = (1 + \varepsilon_2 F) \mathbf{s} + O(\varepsilon^2). \quad (\text{D1})$$

In this setting, we show that the contrast function can only reach its extremum when the variables z_i are independent if choosing the Gaussian kernel. This also helps prove our Theorem 2. We first introduce integral operators corresponding to Gram matrices used as a tool for analysis in Appendix app4.1. In Appendix D 2, an integral operator estimating $\langle \tilde{\mathbf{u}}_{jl}, \tilde{\mathbf{u}}_{ik} \rangle$ is proposed and analyzed in the near-independent setting which gives the value of the inner product.

1. Integral operators

Let $K \in L^2(\mathbb{R} \times \mathbb{R})$ be a symmetric kernel and $f_{z_i}(x) \in L^2(\mathbb{R})$ be the PDF of a random variable z_i . For function $\phi(y) \in L^2(\mathbb{R})$, define several operators mapping from $L^2(\mathbb{R})$ to $L^2(\mathbb{R})$ as follows:

$$\hat{T}_i \phi(y) = \int_{\mathbb{R}} K(x, y) \phi(x) d\rho_{z_i}(x), \quad (\text{D2})$$

$$\hat{I} \phi(y) = \phi(y), \quad (\text{D3})$$

$$\hat{I}_i \phi(y) = \int_{\mathbb{R}} \phi(x) d\rho_{z_i}(x), \quad (\text{D4})$$

$$\hat{K}_i = (\hat{I} - \hat{I}_i) \hat{T}_i (\hat{I} - \hat{I}_i), \quad (\text{D5})$$

where $d\rho_{z_i}(x)$ refers to $f_{z_i}(x)dx$. In particular, use $K'(x,y)$ to write \hat{K}_i concretely by

$$\hat{K}_i\phi(y) = \int_{\mathbb{R}} K'(x,y)\phi(x)d\rho_{z_i}(x). \quad (\text{D6})$$

\hat{K}_i is a Hilbert-Schmidt integral operator and then compact. Then we can talk about the k -th eigenvalues μ_{ik} and eigenfunctions ϕ_{ik} of \hat{K}_i , which is defined by

$$\hat{K}_i\phi_{ik}(x) = \mu_{ik}\phi_{ik}(x). \quad (\text{D7})$$

Nyström method offers an estimate for this equation [45], by replacing the integration on \mathbb{R} by summation on points sampled from the given distribution. For an arbitrary function ϕ , we have

$$\int_{\mathbb{R}} \phi(x)d\rho_{z_i}(x) \approx \frac{1}{N} \sum_{n=1}^N \phi(z_{in}), \quad (\text{D8})$$

where z_{in} are the n -th of all N samples of z_i . Existing analysis on convergency shows that with high probability, the integration can be approximated with precision up to $O(\frac{1}{\sqrt{N}})$ [46]. Use the assumption given in Eq. 15 for simplicity, then we have

$$\mu_{ik}\phi_{ik}(z_{im}) = (\hat{K}_i\phi_{ik})(z_{im}) = \frac{1}{N} \sum_{n=1}^N (K_i(Z))_{mn}\phi_{ik}(z_{in}). \quad (\text{D9})$$

Let $\Phi_{ik} = (\phi_{ik}(z_{i1}), \dots, \phi_{ik}(z_{iN}))^T$, then Eq. D9 can be rewritten as

$$\frac{K_i(Z)}{N}\Phi_{ik} = \mu_{ik}\Phi_{ik}. \quad (\text{D10})$$

This is properly the eigenequation of $K_i(Z)/N$, with eigenvectors Φ_{ik} which can be identified with \vec{u}_{ik} . Nyström method has established a connection between Gram matrices and integral operators from which properties of K_i can be speculated. Conclusions come up in this way that eigenvalues of K_i/N are about μ_{ik} irrelevant to N and decay rapidly which allows a low-rank approximation [31].

2. An operator for the inner product

Define an operator M_{z_i, z_j} :

$$M_{z_i, z_j}(\phi, \psi) = \int_{\mathbb{R}^2} \phi(x)\psi(y)f_{z_i, z_j}(x, y)dxdy, \quad (\text{D11})$$

where f_{z_i, z_j} is the joint PDF of random variables z_i, z_j . It's direct to check that using Nyström method, $M_{z_i, z_j}(\phi_{ik}, \phi_{jl})$ can be approximated by

$$M_{z_i, z_j}(\phi_{ik}, \phi_{jl}) \approx \sum_{m=1}^N \phi_{ik}(z_{im})\phi_{jl}(z_{jm}) = \langle \vec{u}_{ik}, \vec{u}_{jl} \rangle. \quad (\text{D12})$$

We give the expression of $M_{z_i, z_j}(\phi_{ik}, \phi_{jl})$ when z satisfy Eq. D1 in Lemma 6.

Lemma 6. Given $\varepsilon_2^2 \ll \varepsilon_2$, suppose z_i satisfy Eq.D1. For eigenfunction $\phi_{ik}(x)$ defined in Eq. D6, $M_{z_i, z_j}(\phi_{ik}, \phi_{jl})$ equals

$$\varepsilon_2 F_{ij} \int_{\mathbb{R}^2} \phi_{ik}(x)\phi_{jl}(y)(x\frac{\partial}{\partial y} - y\frac{\partial}{\partial x})f_{z_i}(x)f_{z_j}(y)dxdy + O(\varepsilon^2). \quad (\text{D13})$$

Denote by $C_{ik, jl}$ the integration in Eq. D13 and observe the relation

$$\begin{aligned} C_{ik, jl} &\equiv \int_{\mathbb{R}^2} \phi_{ik}(x)\phi_{jl}(y)(x\frac{\partial}{\partial y} - y\frac{\partial}{\partial x})f_{x_i}(x)f_{x_j}(y)dxdy \\ &= - \int_{\mathbb{R}^2} d\rho_{s_i}(x)d\rho_{s_j}(y)(x\frac{\partial}{\partial y} - y\frac{\partial}{\partial x})\phi_{ik}(x)\phi_{jl}(y). \end{aligned} \quad (\text{D14})$$

This relation helps prove that if and only if s_i, s_j are both Gaussian, $C_{ik, jl} = 0$ holds for k, l that satisfy $\mu_{ik}, \mu_{jl} \neq 0$, as stated formally in Lemma 7.

Lemma 7. With the same setting of Lemma 6 and given PDFs f_{s_i} of s_i , if Gaussian kernel is selected, $K(x, y) = \exp\{(x - y)^2/\sigma^2\}$, $C_{ik, jl} = 0$ holds for fixed i, j and all k, l such that $\mu_{ik}, \mu_{jl} \neq 0$ if and only if s_i, s_j are both Gaussian variables.

Lemma. 6 and 7 supports that the Gaussian kernel is an appropriate choice since at least in the near-independent setting, R_K behaves similarly to the mixing coefficients F with such choice, except for Gaussian variables which cannot be separated by ICA inherently [28]. The two proofs are left to Appendix C7 and C8. Moreover, we define $D_{ik, jl}$ as

$$D_{ik, jl}^2 \equiv \int_{\mathbb{R}^2} d\rho_{s_i}(x)d\rho_{s_j}(y)[(x\frac{\partial}{\partial y} - y\frac{\partial}{\partial x})\phi_{ik}(x)\phi_{jl}(y)]^2 - C_{ik, jl}^2, \quad (\text{D15})$$

which is N times the variance of estimating $C_{ik, jl}$ using N samples [47]. Combining Lemma 6 and 7 gives the value of $\langle \vec{u}_{ik}, \vec{u}_{jl} \rangle$.

Corollary 1 (Approximation of inner product). With the same setting of Lemma 6, it holds that

$$|\langle \vec{u}_{ik}, \vec{u}_{jl} \rangle - \varepsilon_2 F_{ij} C_{ik, jl}| < \delta \varepsilon_2 F_{ij} \frac{D_{ik, jl}}{\sqrt{N}}, \quad (\text{D16})$$

with at least probability $1 - 1/\delta^2$.

It is direct by using the Chebyshev inequality.

- [1] C. Jutten and J. Herault, separation of sources, part i: An adaptive algorithm based on neuromimetic architecture, *Signal processing* **24**, 1 (1991).
- [2] P. Comon, Independent component analysis (1992).
- [3] P. Comon, Independent component analysis, a new concept?, *Signal processing* **36**, 287 (1994).
- [4] A. J. Bell and T. J. Sejnowski, Fast blind separation based on information theory, in *Proc. Intern. Symp. on Nonlinear Theory and Applications, Las Vegas* (1995).
- [5] J. Yao, Y. Xiang, S. Qian, S. Wang, and S. Wu, Noise source identification of diesel engine based on variational mode decomposition and robust independent component analysis, *Applied Acoustics* **116**, 184 (2017).
- [6] K. Anand, G. Mathew, and V. U. Reddy, Blind separation of multiple co-channel bpsk signals arriving at an antenna array, *IEEE Signal Processing Letters* **2**, 176 (1995).
- [7] A. Cichocki and W. Kasprzak, Multi-layer neural networks with a local adaptive learning rule for blind separation of source signals, in *Proc. Int. Symp. Nonlinear Theory App., Las Vegas, NV* (Citeseer, 1995).
- [8] M. S. Bartlett, J. R. Movellan, and T. J. Sejnowski, Face recognition by independent component analysis, *IEEE Transactions on neural networks* **13**, 1450 (2002).
- [9] C. J. James and C. W. Hesse, Independent component analysis for biomedical signals, *Physiological measurement* **26**, R15 (2004).
- [10] T. He, G. Clifford, and L. Tarassenko, Application of independent component analysis in removing artefacts from the electrocardiogram, *Neural Computing & Applications* **15**, 105 (2006).
- [11] A. Biton, I. Bernard-Pierrot, Y. Lou, C. Krucker, E. Chapeaublanc, C. Rubio-Pérez, N. López-Bigas, A. Kamoun, Y. Neuzillet, P. Gestraud, *et al.*, Independent component analysis uncovers the landscape of the bladder tumor transcriptome and reveals insights into luminal and basal subtypes, *Cell reports* **9**, 1235 (2014).
- [12] P. Grossmann, O. Stringfield, N. El-Hachem, M. M. Bui, E. R. Velazquez, C. Parmar, R. T. Leijenaar, B. Haibe-Kains, P. Lambin, R. J. Gillies, *et al.*, Defining the biological basis of radiomic phenotypes in lung cancer, *Elife* **6**, e23421 (2017).
- [13] A. Hyvärinen and E. Oja, Independent component analysis: algorithms and applications, *Neural networks* **13**, 411 (2000).
- [14] A. Hyvärinen and E. Oja, A fast fixed-point algorithm for independent component analysis, *Neural computation* **9**, 1483 (1997).
- [15] A. Hyvärinen, Fast and robust fixed-point algorithms for independent component analysis, *IEEE transactions on Neural Networks* **10**, 626 (1999).
- [16] J.-F. Cardoso, High-order contrasts for independent component analysis, *Neural computation* **11**, 157 (1999).
- [17] P. Comon and L. Rota, Blind separation of independent sources from convolutive mixtures, *IEICE Transactions on Fundamentals of Electronics, Communications and Computer Sciences* **86**, 542 (2003).
- [18] A. Taleb and C. Jutten, Source separation in post-nonlinear mixtures, *IEEE Transactions on signal Processing* **47**, 2807 (1999).
- [19] A. W. Harrow, A. Hassidim, and S. Lloyd, Quantum algorithm for linear systems of equations, *Physical review letters* **103**, 150502 (2009).
- [20] A. Kandala, A. Mezzacapo, K. Temme, M. Takita, M. Brink, J. M. Chow, and J. M. Gambetta, Hardware-efficient variational quantum eigensolver for small molecules and quantum magnets, *Nature* **549**, 242 (2017).
- [21] G. H. Low and I. L. Chuang, Optimal hamiltonian simulation by quantum signal processing, *Physical review letters* **118**, 010501 (2017).
- [22] A. M. Childs, Universal computation by quantum walk, *Physical review letters* **102**, 180501 (2009).
- [23] P. W. Shor, Polynomial-time algorithms for prime factorization and discrete logarithms on a quantum computer, *SIAM review* **41**, 303 (1999).
- [24] M. A. Nielsen and I. Chuang, *Quantum computation and quantum information* (2002).
- [25] L. K. Grover, Quantum mechanics helps in searching for a needle in a haystack, *Physical review letters* **79**, 325 (1997).
- [26] S. Lloyd, M. Mohseni, and P. Rebentrost, Quantum principal component analysis, *Nature Physics* **10**, 631 (2014).
- [27] J. V. Stone, Independent component analysis: an introduction, *Trends in cognitive sciences* **6**, 59 (2002).
- [28] P. Comon and C. Jutten, *Handbook of Blind Source Separation: Independent component analysis and applications* (Academic press, 2010).
- [29] L. K. Grover, A framework for fast quantum mechanical algorithms, in *Proceedings of the thirtieth annual ACM symposium on Theory of computing* (1998) pp. 53–62.
- [30] S. Subramanian and M.-H. Hsieh, Quantum algorithm for estimating α -renyi entropies of quantum states, *Physical review A* **104**, 022428 (2021).
- [31] F. R. Bach and M. I. Jordan, Kernel independent component analysis, *Journal of machine learning research* **3**, 1 (2002).
- [32] P. Drineas, M. W. Mahoney, and N. Cristianini, On the nyström method for approximating a gram matrix for improved kernel-based learning., *journal of machine learning research* **6** (2005).
- [33] A. Edelman, T. A. Arias, and S. T. Smith, The geometry of algorithms with orthogonality constraints, *SIAM journal on Matrix Analysis and Applications* **20**, 303 (1998).
- [34] V. Giovannetti, S. Lloyd, and L. Maccone, Quantum random access memory, *Physical review letters* **100**, 160501 (2008).
- [35] L. Ruiz-Perez and J. C. Garcia-Escartin, Quantum arithmetic with the quantum fourier transform, *Quantum Information Processing* **16**, 1 (2017).
- [36] A. Gilyén, Y. Su, G. H. Low, and N. Wiebe, Quantum singular value transformation and beyond: exponential improvements for quantum matrix arithmetics, in *Proceedings of the 51st Annual ACM SIGACT Symposium on Theory of Computing* (2019) pp. 193–204.
- [37] S.-i. Amari, A. Cichocki, and H. Yang, A new learning algorithm for blind signal separation, in *Advances in Neural Information Processing Systems*, Vol. 8, edited by D. Touretzky, M. Mozer, and M. Hasselmo (MIT Press, 1995).
- [38] J. Himberg and A. Hyvarinen, Icasso: software for investigating the reliability of ica estimates by clustering and visualization, in *2003 IEEE XIII Workshop on Neural Networks for Signal Processing (IEEE Cat. No.03TH8718)* (2003) pp. 259–268.
- [39] Q. T. Nguyen, B. T. Kiani, and S. Lloyd, Block-encoding dense and full-rank kernels using hierarchical matrices: applications in quantum numerical linear algebra, *Quantum* **6**, 876 (2022).
- [40] T. Li, X. Wang, and S. Zhang, A unified quantum algorithm framework for estimating properties of discrete probability distributions, *arXiv preprint arXiv:2212.01571* (2022).
- [41] N. Delfosse and P. Loubaton, Adaptive blind separation of independent sources: a deflation approach, *Signal processing* **45**, 59 (1995).

- [42] T. Li and X. Wu, Quantum query complexity of entropy estimation, *IEEE Transactions on Information Theory* **65**, 2899 (2018).
- [43] R. Bhatia, *Matrix analysis*, Vol. 169 (Springer Science & Business Media, 2013).
- [44] S. K. Godunov, A. Antonov, O. Kiriljuk, and V. Kostin, *Guaranteed accuracy in numerical linear algebra*, Vol. 252 (Springer Science & Business Media, 2013).
- [45] K. Atkinson and W. Han, *Theoretical numerical analysis*, Vol. 39 (Springer, 2005).
- [46] L. Rosasco, M. Belkin, and E. De Vito, On learning with integral operators., *Journal of Machine Learning Research* **11** (2010).
- [47] D. J. C. Mackay, Introduction to monte carlo methods, in *Learning in Graphical Models*, edited by M. I. Jordan (Springer Netherlands, Dordrecht, 1998) pp. 175–204.